A far infrared laser sideband spectrometer in the frequency region 550–2700 GHz

P. Verhoeve, E. Zwart, M. Versluis, M. Drabbels, J. J. ter Meulen, W. Leo Meerts, and A. Dymanus

Fysisch Laboratorium, Katholieke Universiteit Nijmegen, Toernooiveld, 6525 ED Nijmegen, The Netherlands

D. B. McLay

Stirling Hall, Queen's University, Kingston K7L 3Y7, Canada

This paper describes a tunable far-infrared (FIR) spectrometer. Tunable radiation is obtained by frequency mixing, fixed frequency FIR laser radiation and tunable microwave radiation in Schottky barrier diodes. An optically pumped laser and an HCN discharge laser are used as FIR sources and klystrons in the frequency range of 22–114 GHz as microwave sources. This yields an 85% coverage of the frequency region between 550 and 2700 GHz. Up to sixth order sidebands have been generated and used for spectroscopy. The ultimate sensitivity corresponds to a minimum detectable fractional absorption of 10^{-5} at 1-s RC time. The applicability of the spectrometer in high-resolution spectroscopy of transient species has been demonstrated by the observation of spectra of OD and N_2H^+. New laser emissions of optically pumped CH_2F_2 have been found and accurate frequencies have been determined for some of them.

I. INTRODUCTION

High-resolution far-infrared (FIR) spectroscopy has long been hindered by the lack of continuously tunable sources of coherent radiation. The extension of microwave techniques by generation of harmonic frequencies[1] and the use of backward wave oscillators[2] do not reach far beyond the 1-THz mark. The introduction of laser sideband spectrometers,[3,4] based on the mixing of radiation of fixed frequency lasers and tunable microwave generators in Schottky barrier diodes, opened the possibility of sensitive spectroscopy at higher frequencies. This technique was developed simultaneously in Nijmegen,[3] with an HCN laser as FIR source, and at MIT,[4] with an optically pumped HCOOH laser as FIR source. The Nijmegen spectrometer has been modified and improved over the years and although it has been used successfully for the observation of spectra of several free radicals and small molecular ions, its details have never been well documented.

In recent years, this technique has been spreading out and other groups have constructed similar spectrometers. They all have in common the use of optically pumped FIR lasers and Schottky barrier diodes mounted in open structure mixers[5] for a quasi-optical coupling of FIR radiation to the diode. Differences occur in the sources of microwave radiation, in the coupling of microwaves to the diode, in the detection system, and in the way sidebands are separated from the fundamental laser radiation. Farhoomand *et al.*[6] and our group[7] use klystrons with frequencies up to 114 GHz and coupling to the mixer via waveguides in which the diode is mounted. The Berkeley group[8] uses frequency synthesizers and multipliers, yielding frequencies up to 75 GHz; coupling is performed with transmission lines (up to 45 GHz) or waveguides (higher frequencies). The Lille group[9] uses a YIG oscillator (2–4 GHz) coupled coaxially to the diode. The latter spectrometer differs from the other three in the application of heterodyne detection instead of bolometers, a system that does not require a rigorous separation of sidebands from the fundamental laser radiation as is the case with bolometer detection. Good separation is achieved with polarizing diplexers in combination with Fabry-Perot interferometers[6,8] or a nonpolarizing diplexer in combination with a grating monochromator.[7] All four spectrometers have comparable sensitivities in the 1-THz region, corresponding to a minimum detectable fractional absorption of 10^{-5}. Two of them[6,9] are operated at frequencies up to 3 THz, whereas the other two[7,8] have been used near 1 THz, until now.

Evenson *et al.*[10] have introduced the generation of tunable FIR radiation by mixing the output of two waveguide CO_2 lasers, one of which is tunable, in metal-insulator-metal (MIM) diodes. This technique has been applied in spectroscopy at frequencies up to 5 THz.[11] A more detailed comparison of all five spectrometers can be found in Ref. 12.

In this article we describe the present state of the Nijmegen laser sideband spectrometer, originally built by Bicanic *et al.*[3] who used a triple-arm waveguide mixer. Van den Heuvel *et al.* improved the coupling of FIR radiation with the use of an open structure mixer, which yielded a sensitivity sufficient to detect spectra of molecular ions.[13] We have now extended the frequency range of the spectrometer to 2.7 THz with the addition of an optically pumped FIR laser to the previously used HCN discharge laser. This has enabled us to study the ground-state inversion spectrum of the hydronium ion H_3O^+ at 1.6 THz. Results of this work have been published elsewhere.[14]

A schematic view of the experimental setup is shown in Fig. 1. FIR laser radiation with fixed frequency f_l and tuna-
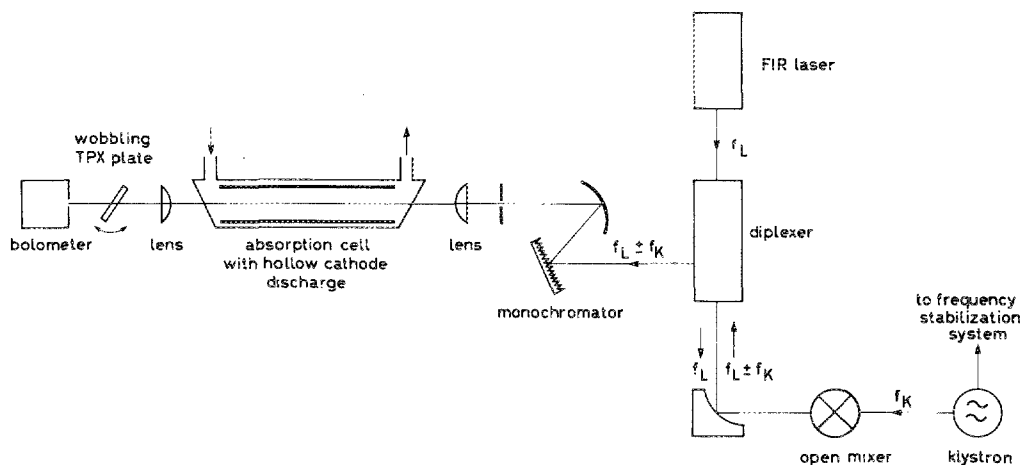
FIG. 1. Schematic view of the FIR laser sideband spectrometer.

ble microwave radiation with frequency f_k are fed into a Schottky barrier diode mounted in an open structure mixer. In a nonlinear process, sideband frequencies f_s are generated which are given by

$$f_s = f_l \pm n f_k, \quad n = 1,2,3,\dots . \tag{1}$$

These frequencies are reradiated by the mixer in a beam anti-parallel to the incoming laser radiation. This beam consists, however, mainly of reflected fundamental laser radiation. The latter is suppressed by the diplexer that separates frequencies f_l and f_s by interferometric techniques. A grating monochromator provides selection of one sideband and further suppression of laser radiation. The monochromatic beam of tunable FIR radiation passes through a discharge cell that enables studies of transient species and is finally detected with a sensitive bolometer.

The various components of the spectrometer are described in detail in the following sections. The performance of the system is discussed and some examples of application in spectroscopy are given.

II. LINE TUNABLE FAR INFRARED LASERS

A. Lasers used in the present experiment

The monochromatic far-infrared radiation required for the generation of tunable radiation is provided by two sources: (1) an HCN discharge laser and (2) an optically pumped laser. The HCN laser has been used successfully for many years, thanks to its high power, stability, and low noise level. Details of construction and operation of this laser have been described extensively before.[15] The relevant features in this context are the emitted frequencies and power levels; the HCN laser is operated at either 890760.3 or 964312.7 MHz with 50- and 20-mW output power, respectively. This enables spectroscopy in the region around 0.9 THz.

Recently, we have constructed an optically pumped FIR laser in order to extend this frequency range. Such a laser can be operated at a large number of frequencies, in the range of 0.2 to over 10 THz. This requires the use of different gain media of which CH_3OH and $HCOOH$ are perhaps the best known. Unlike the HCN laser, where an electric discharge creates the required population inversion in the gain

medium, this is brought about by radiative excitation in an optically pumped laser. In most cases, molecules are vibrationally excited with an IR laser and then FIR laser action occurs between two rotational levels in the excited vibrational state. Optically pumped FIR laser action was first observed by Chang and Bridges[16] in CH_3F and the first optically pumped FIR waveguide laser was used by Hodges and Hartwick.[17] A review of optically pumped far-infrared lasers can be found in Ref. 18. An extensive list of available far-infrared laser frequencies is given in Ref. 19, but it should be noted that many new frequencies have been found recently, especially with isotopic species of the conventional gain media for the FIR laser as well as for the IR pump laser.

B. Construction details of the optically pumped FIR laser

For the purpose of the present experiment, it is important to have high output power of the laser at as many frequencies as possible. The most favorable setup to achieve this is a laser with a dielectric waveguide. In this case the cavity mode with the lowest propagation losses is usually the EH_{11} mode. This mode is also preferentially excited if the laser is axially pumped and couples very efficiently into the TEM_{00} free-space mode,[20] thus yielding a FIR beam with a Gaussianlike shape. Therefore, an optically pumped FIR waveguide laser has been constructed. The FIR cavity is built around a 385-cm-long quartz waveguide with an inner diameter of 32 mm. The tube is constructed from four equally long parts. The inner wall is somewhat irregular at the weldings which might affect the performance. The inner diameter was chosen to match the desired wavelength region of 500–100 μm (in frequency units: 600–3000 GHz or 20–100 cm^{-1}). Theoretically,[21] the gain in a waveguide laser is inversely proportional to its radius α, whereas propagation losses are proportional to λ^2/α^3, where λ is the FIR wavelength. Consequently, there is an optimum radius for each FIR emission and the choice of a certain value for α implies an upper limit for the wavelength that can oscillate. In our case the 742.6 μm emission of CH_3OH pumped by the 9R(40) line of the CO_2 laser has been observed to oscillate, which is well beyond our requirements. On the other hand,

loss of pump power at the waveguide walls is expected to increase with decreasing diameter since the IR pump beam is diverging along the tube. In practice, Hodges et al.[22] found the output power at the 118.8-μm emission of CH_3OH to be roughly independent of the diameter for diameters of 10–30 mm at a cavity length of 0.8 m. The length of the waveguide was chosen in view of the desired high output power. An increase in FIR power proportional to the length of the tube up to 3–4 m has been observed for FIR emissions with small absorption coefficients at the appropriate pump wavelengths.[22,23]

The waveguide is placed between two plane gold-coated brass mirrors with a diameter of 50 mm. Both mirrors are within 5 mm from the edges of the tube. Losses originating from the coupling of the EH_{11} waveguide mode to the TEM_{00} free-space mode and vice versa can be shown to be negligible for these distances.[20] The mirrors have central holes, 1.5 mm at the end where the IR beam is injected into the cavity and 5 mm at the other end where the FIR radiation is extracted. Larger output coupling holes were not used in order to keep the IR power escaping from the cavity at reasonably low levels. Still, some 15% of the IR power was observed to leave the cavity through the 5-mm hole. Separation of the IR radiation from the FIR power is accomplished with a crystalline quartz vacuum window (thickness 4 mm) mounted behind the outcoupling hole. Crystalline quartz is a very good absorber for IR and reasonably transparent for FIR (absorption coefficient $\alpha \approx 0.45$ cm^{-1} at $\lambda = 200\,\mu$m). The problem of the loss of IR radiation can be overcome by using a hybrid output coupler introduced by Hodges et al.[23] Instead of a gold-coated brass mirror with a central hole, a crystalline quartz plate is used. This plate is slightly wedged to prevent interfering reflections between the surfaces at certain wavelengths and the optical axis of the crystal is perpendicular to the surface to avoid birefringence. It is coated with a multilayer dielectric coating which is highly reflective at IR wavelengths and transparent for FIR. On top of this, a gold coating is deposited with a 10-mm central hole. Indeed, the use of such an output coupler yielded a 50% higher output power for the strong CH_2F_2 laser lines. However, it was easily damaged by 50 W of IR power and therefore, conventional hole couplers have been used in most experiments.

Dielectric shims for supporting and aligning the tube are placed at four equidistant positions along the waveguide. These proved to be very important for the optimization of the output power of each individual laser line. Initial alignment of the cavity is performed by shining a He-Ne laser beam along its axis and centering the diffraction patterns from the holes in the mirrors. After evacuation of the system, the orientation of both mirrors can be adjusted to optimize laser output. The laser cavity length can be tuned by means of a spring-loaded "pantograph" assembly driven by a micrometer screw. This assembly allows a maximum translation of 5 mm for the output coupling mirror. Both mirror mountings are held in aluminum boxes to which also the gas inlet tube, vacuum gauge, and vacuum pump connection are attached. Vacuum is maintained by a 16 m^3/h rotary pump, yielding an ultimate pressure in the laser of about 1 Pa. A

zeolite filter is placed in the pumping line to prevent contamination of mirrors and waveguide by oil. The entire cavity is mounted in a frame of four 4-m-long invar rods. These provide an adequate stabilization of the cavity length against temperature variations.

The laser is pumped by a line tunable CO_2 laser (Apollo Lasers Inc., model 150) with a maximum single line power of 150 W. The CO_2 laser is equipped with a piezoelectric translator with which its frequency can be tuned into resonance with the absorption frequency of the gain medium of the FIR laser. No active stabilization of this frequency is applied. The IR beam is coupled into the FIR cavity and carefully aligned along the axis by means of three external mirrors. Two ZnSe lenses with focal lengths of 38 and -19 cm, positioned, respectively, at 40 and 12.5 cm from the hole in the incoupling mirror, form a beam that slowly diverges along the waveguide and hits the wall in the second half of the tube, thus preventing excessive local heating of the waveguide. The second lens also serves as a vacuum seal for the FIR laser. For maximum FIR output power, a good Gaussian shape for the incident IR beam proved to be very important, as was also found by Hodges et al.[22] An increase of about 50% in FIR power at the same pump power was observed when the initially used Edinburgh PL3 CO_2 laser with a ring-shaped beam was replaced by the Apollo 150 CO_2 laser. To the present time, pump powers have been limited to 60 W or less to avoid damage to the uncooled FIR cavity.

C. Performance of the optically pumped FIR laser

So far the laser has been operated with only four different gain media: CH_3OH, $HCOOH$, CH_2F_2, and CH_3OD. These gases provide about 20 strong laser emissions in the 600–2000 GHz frequency region. They are listed in Table I; frequencies are taken from Ref. 19 unless indicated otherwise (see Sec. II D) and relative strengths, denoted with W (weak), M (medium), and S (strong) are measured with a pyroelectric detector that was not calibrated for FIR wavelengths. The absolute powers are estimated to range between 10 and 100 mW for pumping powers up to 50 W. The dependence of FIR power on IR between 20 and 60 W is essentially linear and suggests a further increase in FIR power with increasing CO_2 laser power. At most FIR wavelengths, several transverse modes are excited. The shorter the wavelength, the more modes will reach threshold since propagation losses are proportional to λ^{-2}.

For better stability of the output power, the laser is used with a slowly flowing gain medium except in case of the expensive CH_2F_2. The output power has been observed to be constant within a few percent for periods of 20–30 min.

The FIR beam leaving the laser is slightly diverging due to diffraction at the output coupling hole. The diameter w of the beam (Airy disk) is given by $w = 1.22\,(\lambda/b)L$, where L is the distance from the hole, b is the radius of the hole, and λ is the wavelength. Figure 2 shows a cross section of the beam for $\lambda = 118.8\,\mu$m, $L = 20$ cm, and $b = 2.5$ mm. As can be seen, the beam has a Gaussianlike power distribution. The diverging FIR beam is collimated by a polyethylene lens

TABLE I. Strong optically pumped FIR laser emissions.

Gain medium	Frequency in MHz[a]	Polarization	Pump line CO$_2$ laser	Relative strength
HCOOH	584 372.9	‖	9R(28)	M
HCOOH	692 951.4	‖	9R(20)	M
HCOOH	716 156.8	‖	9R(22)	M
HCOOH	761 607.7	‖	9R(18)	M
CH$_2$F$_2$	1 042 150.4	‖	9R(34)	M
CH$_3$OH	1 193 727.3	‖	10R(38)	W
CH$_2$F$_2$	1 267 131.0	‖	9R(06)	M
CH$_2$F$_2$	1 300 334.3[b]	⊥	9R(34)	M
CH$_2$F$_2$	1 302 845.8	⊥	9R(42)	W
CH$_2$F$_2$	1 397 118.6	⊥	9R(34)	S
CH$_2$F$_2$	1 530 849.9[b]	⊥	9R(32)	S
CH$_2$F$_2$	1 546 083.4	‖	9R(22)	M
CH$_2$F$_2$	1 562 655.9	‖	9P(22)	W
CH$_2$F$_2$	1 626 602.6	⊥	9R(32)	S
CH$_3$OH	1 838 839.3	‖	10R(38)	M
CH$_2$F$_2$	1 891 274.2	‖	9P(10)	M
CH$_2$F$_2$	2 216 263.5[c]	‖	9P(24)	M
CH$_2$F$_2$	2 237 296.4[c]	⊥	9P(22)	W
CH$_2$F$_2$	2 447 968.5[c]	⊥	9R(22)	S
CH$_3$OH	2 522 781.6	‖	9P(36)	S
CH$_2$F$_2$	2 546 495.0[c]	⊥	9R(20)	S
CH$_3$OD	2 557 365.4	‖	9P(26)	M

[a] From Ref. 19.
[b] See Sec. II D.
[c] From Ref. 47.

between the laser and the diplexer.

The FIR laser radiation is linearly polarized and the direction of polarization with respect to the CO$_2$ pump laser beam depends on the rotational quantum numbers J of the energy levels involved in the pumping process and laser action: if ΔJ(pump) $+ \Delta J$(FIR) is even (odd), both polarizations are parallel (perpendicular) to each other (compare Fig. 4). These relative polarizations (given in Table I for the individual laser lines) are relevant because the mixer (Sec. III B) and the diplexer (Sec. IV A) allow only one direction of polarization, which is suitably obtained by the proper use of mirrors between laser and diplexer.

D. New laser lines of ^{12}CH$_2$F$_2$

In the course of spectroscopic work near 1540 GHz, we encountered an unknown laser emission oscillating simulta-

neously with the 1626.6-GHz line of ^{12}CH$_2$F$_2$, pumped by the 9R(32) line of the ^{12}C^{16}O$_2$ laser, and causing noisy sideband power. Analysis of the laser output by means of a Fabry-Perot interferometer showed oscillation at two more frequencies besides the 1626.6-GHz line. A similar analysis of other strong lines of CH$_2$F$_2$ yielded two additional frequencies at the 9R(34) and one additional frequency at the 9R(20) pump lines. Figure 3 shows the Fabry-Perot interferogram (at fixed laser cavity length) of the FIR laser pumped by the 9R(32) line. The different wavelengths are separately indicated on the bars below the interferogram. From this scan, the ratio of the wavelengths was obtained and, using the known frequency of the strongest component, the frequencies of the new lines could be determined within a few GHz. A more accurate value for the frequency could be found if the line was strong enough to generate sufficient sideband power for spectroscopic measurement. In this case, absorption lines of D$_2$O or H$_2$O with known frequencies[24] could be detected, which enabled us to derive the laser frequency with an accuracy of 6 MHz. A final improvement was achieved by measuring the same absorption line with both the unknown laser line and a known laser line. The uncertainty in the laser frequencies determined in this way is estimated to be 2 MHz. The newly found and the known laser lines are listed in Table II together with their relative strengths. Three of the new lines have been reported by other authors,[25–27] but mostly with large uncertainties in their frequencies. The values from these authors are listed in the last column of Table II.

It is seen that the frequency difference between successive lines produced by the same pump line is always approximately 96 GHz, which is about twice the rotational A constant of CH$_2$F$_2$.[28] This strongly suggests that these laser emissions originate from a cascade process in the excited vibrational state. Using the tentative assignments for the levels involved with the known laser lines,[29] we assigned the levels involved with the new lines. These assignments are also given in Table II. A energy level scheme showing the complete set of laser emissions associated with the 9R(32) pump line is drawn in Fig. 4.

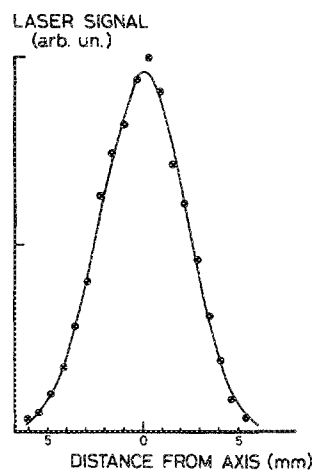Further arguments in favor of a cascade process are the facts that the new lines are always found oscillating simulta-
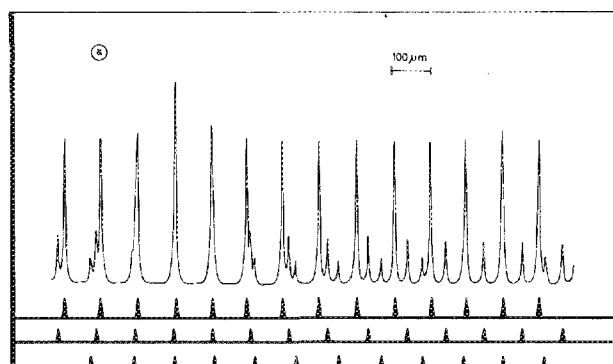

FIG. 2. Spatial power distribution in the FIR beam ($\lambda = 118.8 \mu$m) at 20 cm from the output coupling hole (diameter 5 mm).

FIG. 3. Fabry-Perot interferogram of the CH$_2$F$_2$ FIR laser output when pumped by 9R(32). The strongest line represents the well-known laser line of 1626.6 GHz whereas the other lines are cascade emissions.

TABLE II. Frequencies and tentative assignments of new laser emissions of $^{12}CH_2F_2$ pumped by the $^{12}C^{16}O_2$ laser.

Pump line and exc. vibration	Observed FIR laser frequency in MHz	Proposed assignment (J,K_a,K_c)	Relative strength	Previous observations, in GHz
9R(32)	1 626 602.6(1.5)[a]	18,17,1→17,16,2[b]	100	1626.6048(20)[c]
ν_9	1 530 849.9(2.0)	17,16,2→16,15,1	40	1530.8487(12)[c]
	1 434 872.9(2.0)	16,15,1→15,14,2	6	
9R(34)	1 397 118.8(1.5)[a]	18,14,4→17,13,5[b]	100	1399.3(0.7)[d]
ν_9	1 300 334.3(2.0)	17,13,5→16,12,4	46	1302.3(0.8)[d]
	1 206 200(5000)	16,12,4→15,11,5	2	1205.0(2.4)[d]
9R(20)	2 546 495(1.5)[a]	38,23,15→37,22,16[b]	100	
$\nu_4 + \nu_9$	2 453 400(5000)	37,22,16→36,21,15	10	

[a] From Ref. 19, known frequencies.
[b] From Ref. 29.
[c] From Ref. 27.
[d] From Ref. 25.

neously with the strong line and have the same polarization with respect to the pump line as the strong line.

A striking feature of the newly found laser lines is their strength. This makes them a welcome extension of the spectral range of the spectrometer.

III. THE GENERATION OF SIDEBANDS

A. The microwave system

Microwave radiation is supplied by a set of klystrons that completely covers the frequency region of 22 to 114 GHz. Two types of klystrons are used: OKI (V10 or V11) below 85 GHz and Varian (VRB series) above this frequency. Each individual klystron has a tuning range of approximately 5 GHz. Typical power levels are estimated to be 100 mW. Three waveguide systems are used to cover this region: WR-28 for 22–40 GHz, WR-15 for 40–70 GHz, and WR-10 for 70–115 GHz.

Microwave frequencies are stabilized and controlled by a phase-lock system. Above 40 GHz the klystrons are locked to a K-band klystron (17–27 GHz) which, in its turn, is locked to a HP 8660B frequency synthesizer (<1 GHz). Below 40 GHz, klystrons are directly locked to this synthesizer. This device is itself locked to a Rb frequency standard, assuring a frequency accuracy well within the experimental requirements. Automatic external control of the frequency synthesizer enables an electrical tuning of the microwave frequency via the phase-lock system. Every few hundred MHz, the klystrons have to be mechanically tuned to keep them near the centers of their modes.

B. The mixer

The open structure mixer used in the present investigations is essentially the same as the one used by van den Heuval et al.[30] A schematic view of its relevant features is shown in Fig. 5. The chip containing an array of Schottky barrier diodes is soldered on a golden pin (diameter 0.6 mm), that is mounted in a rectangular waveguide. This waveguide is either WR-12 for the higher microwave frequencies (>50 GHz) or WR-28 for the lower frequencies. If necessary, tapered waveguide sections are used to connect the mixer to the waveguide systems described above. The cutoff frequency of the WR-28 waveguides is 21.1 GHz which sets the
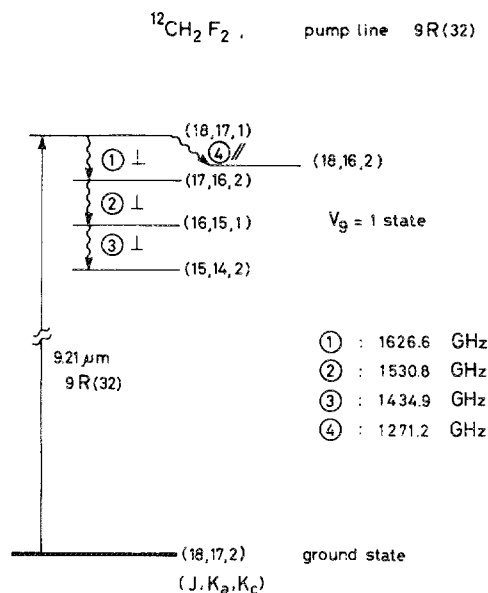
$^{12}CH_2F_2$, pump line 9R(32)

FIG. 4. Laser lines of CH_2F_2 pumped by 9R(32). Frequencies 2 and 3 are newly found. The symbols $\perp$ and $\parallel$ refer to the direction of polarization of FIR radiation with respect to IR pump beam.
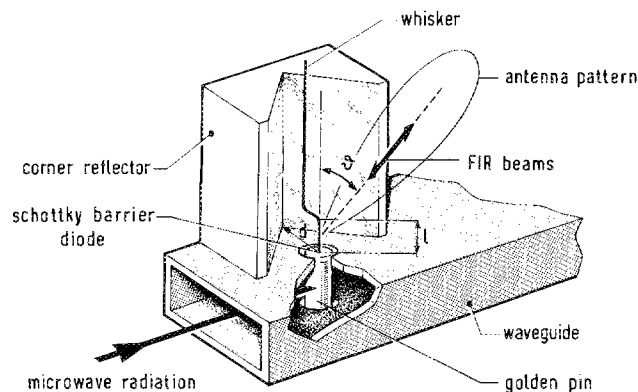

FIG. 5. Schematic view of the open structure mixer.

lower limit for the microwave frequencies that can be used. The golden pin acts as an antenna for the incoming microwaves, but the coupling of microwaves to the diode is improved if the chip is positioned just inside the waveguide. The upper waveguide wall is made as thin as possible (≈ 0.1 mm) in order not to disturb the coupling of FIR radiation to the diode (see below). The holes in the waveguide walls are 1 mm in diameter. The waveguide is terminated by a movable plunger with which the coupling of microwave radiation to the diode can be optimized. This plunger was also seen to influence slightly the coupling of FIR laser radiation to the diode.

The actual diode contact is established by making a point contact with a gold-coated tungsten whisker (≈ 8 mm long, 25 μm diameter) on one of the diodes on the chip. The whiskers are electrolytically etched (5% $K_4[Fe(CN)_6]3H_2O$, 5% NaCN) to obtain tips of ≈ 1 μm diameter, i.e., smaller than the diameter of the Schottky barrier diodes. The whisker is held in a spring-loaded frame with screw mechanisms that allow careful maneuvering of the whisker tip towards the chip and making a contact. This procedure is performed under a stereo microscope. The result is checked by looking at the oscilloscope trace of the I-V curve of the diode. Usually the sharpness of the bend in the nonlinear part of this curve is a good indication for the quality of the contact. The golden pin on which the chip is soldered, is insulated from the rest of the mixer and connected to a BNC plug. Via this plug, a bias voltage can be applied to the diode and its I-V curve can be monitored.

FIR radiation is focused on the whisker by means of a gold-coated off-axis paraboloidal reflector (focal length 60 mm, distance optical axis-mechanical axis 80 mm). For efficient coupling, it is important to mount the whisker parallel to the direction of polarization of the incoming radiation. Only the lower part of the whisker (see Fig. 5) acts as a long wire antenna[31] and the antenna length is well defined by a sharp double bend in the whisker.[32] The antenna pattern is greatly improved by the use of a corner reflector behind the whisker. With the proper choice of antenna length l and distance d between the vertex of the corner reflector and the whisker (at a given wavelength λ), the cylindrically symmetric antenna pattern of the free standing antenna can be compressed into a single lobe around an axis in the plane of the whisker and the vertex of the corner reflector.[5,33] This lobe is indicated in Fig. 5. The angle Θ depends on the ratio[31] l/λ. A favorable configuration is $l = 4\lambda$ with corresponding $\Theta \approx 25°$ and $d = 1.2\lambda$ with a 90° opening angle of the corner reflector.[5] Efficient coupling of FIR radiation is achieved if the cone of the focused radiation coincides with the lobe of the antenna pattern. Since this pattern is identical for both reception and emission, the generated tunable FIR radiation is emitted within the same lobe and collected efficiently by the paraboloidal reflector.

The mixer mount is provided with three micrometer screws for x-y-z translation of the complete mixer and thus the antenna part of the mixer can be positioned in the focus of the paraboloidal reflector. Furthermore, the angle Θ and distance d can be continuously varied. For ease of operation the antenna length l is not especially adapted to the exact

wavelength of the current experiment, but always kept at 1–1.5 mm. In practice, the optimum setting of all parameters is found by maximizing the rectified laser signal from the diode.

C. Schottky barrier diodes

The present spectroscopic experiments were performed with two types of Schottky barrier diode chips, listed in Table III. For several years, chips obtained from Fetterman (MIT, MA) have been used in the 1-THz region. When their performance was observed to deteriorate, they were replaced by the model SD-018 mixer diodes from Farran Technology Limited. These were used in most experiments above 1 THz. Recently we obtained the model 117 diodes from the Semiconductor Device Laboratory of the University of Virginia (Charlottesville, VA), but these have not yet been tested extensively. A simple equivalent scheme of a Schottky barrier diode is shown at the right hand side of Fig. 6. Herein, R_j is the nonlinear resistance of the barrier, R_s is the spreading resistance of the diode, and C_j is the parasitic capacitance of the barrier. The values of R_s and C_0 (the zero bias value of C_j) determine the high-frequency performance of the diode. A convenient number to use is the cutoff frequency $f_0 = (2\pi R_s C_0)^{-1}$. Both R_s and C_0 depend on the radius of the barrier.[34] The value of C_j depends on the bias voltage applied and since $C_j \geqslant C_0$ (Ref. 34) the actual value of the cutoff frequency f_c is smaller than f_0. The relevant parameters of the three types of diodes are listed in Table III. Comparable results for generated sideband powers below 1 THz were obtained with the first two diodes as could be expected from their specifications. The third diode has a higher value of f_0, suggesting better performance at higher frequencies. Indeed, in preliminary tests, a three times higher sideband power level at 2.5 THz has been observed with these diodes than with the SD-018 diodes. No significant improvement was observed at 1.5 THz.

The I-V characteristics with and without incident radiation are shown in Fig. 6. The diodes are operated in the nonlinear part of the I-V curve by applying a bias voltage of ≈ 0.8 V. At this value the rectified laser signal is maximum. Since the I-V curve is severely distorted when microwave radiation is coupled to the diode (see Fig. 6), a different optimum value of the bias voltage is expected for generation of sidebands. This effect has clearly been seen for the first sideband [$n = 1$ in Eq. (1)]: an increase in microwave power requires a higher bias voltage for maximum sideband sig-

TABLE III. Schottky barrier diodes.

Diode	R_s (Ω)	C_0 (fF)	Diameter (μm)	f_c (THz)
MIT[a]	≈ 15	≈ 2	≈ 1.5	≈ 5.3
SD-018[b]	11	≈ 2.2	≈ 2	6.5
117[c]	12	1.2	≈ 2	11.0

[a] Data from Ref. 34.
[b] Data from test report from Farran Technology Ltd.
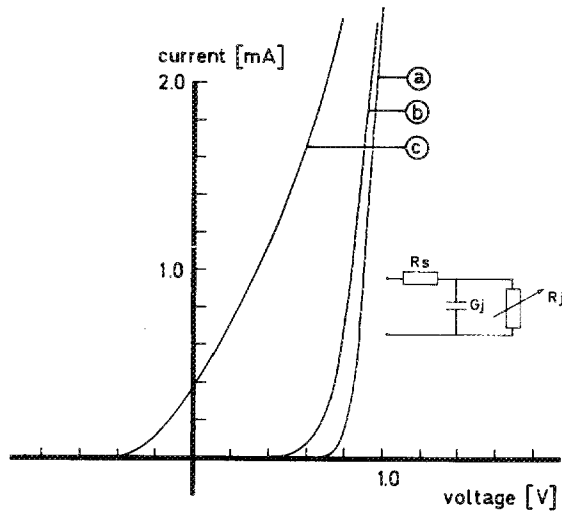[c] Data from test report from Virginia University.

FIG. 6. *I-V* curves of a Schottky barrier diode: (a) without incident radiation, (b) with incident FIR laser radiation, and (c) with incident microwave radiation. Right: equivalent scheme of a Schottky barrier diode. R_s and C_j are diode parasitics, R_j is the nonlinear resistance.

nal. The higher order sidebands ($n = 2,3,...$) show a more complicated dependence on the bias voltage as is shown in Fig. 7. Generally, the sidebands with even n require lower bias voltages than those with odd n. A similar behavior was observed by Sanchez et al.[35] in infrared-microwave mixing experiments with metal-to-metal point contact diodes. It was attributed to the dependence of the different order mixing signals on the corresponding order of the derivative of the *I-V* characteristic of the diode.

IV. WAVELENGTH SELECTING ELEMENTS

The radiation emitted by the mixer antenna contains several frequencies according to Eq. (1). By far the strongest, however, is the radiation at the fundamental laser frequency, reradiated and reflected by the mixer in the same direction. There is a difference of three to four orders of magnitude in power level between laser power and sideband power. It is extremely important to suppress the former, because its presence would completely obscure the sidebands and greatly reduce the sensitivity of the system due to addi-
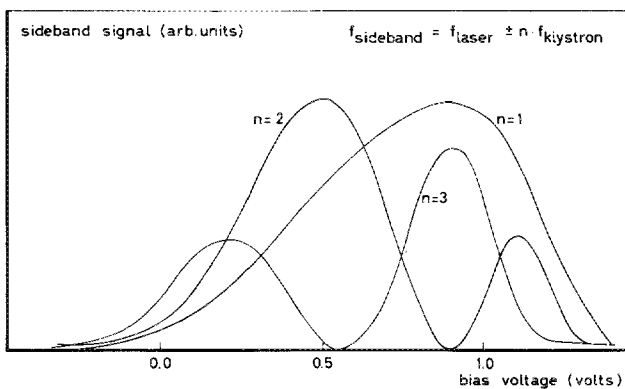

FIG. 7. Bias voltage dependence of the various order sideband signals. The relative strengths of the three sidebands are not on scale.

tional noise at the detector. For this purpose two wavelength selecting elements are used: a diplexer and a grating monochromator (see Fig. 1).

A. The diplexer

The diplexer is positioned between laser and mixer. This device, originally used by Erickson,[36] is essentially a Michelson-type interferometer consisting of two gold-coated corner reflectors (one movable) and a beam splitter. It provides a spatial separation of sidebands and fundamental laser radiation from the same beam. Figure 8 shows the paths of the beams involved through the diplexer. The transmission of laser radiation from laser (L) to mixer (M) and of laser or sideband radiation from mixer to detector (D) can be calculated from:

$$T_{LM}(\lambda) = 2R(1 - R)[1 + \cos(2\pi x/\lambda)] \qquad (2a)$$

and

$$T_{MD}(\lambda) = 1 - 2R(1 - R)[1 + \cos(2\pi x/\lambda)], \qquad (2b)$$

where R is the multiple beam power reflection coefficient of the beam splitter, x is the path difference in the two arms of the diplexer, and λ is the wavelength of laser or sideband radiation. Lossless transmission of both laser and sidebands, i.e., $T_{LM}(\lambda_l) = 1$ and $T_{MD}(\lambda_s) = 1$, can be achieved if $R = 0.5$ and with a proper setting of x: $x = (p + 1/2)\lambda_s = q\lambda_l$ with p and q integers. This simultaneously yields a complete suppression of laser radiation in the direction of the detector: $T_{MD}(\lambda_l) = 0$. It should be noted that both sideband frequencies $f_s = f_l \pm f_k$ are transmitted at the optimum setting of x.

The sideband power generated at the mixer is proportional to the incoming laser power and thus, for $R = 0.5$, the sideband power at the detector is given by

$$T_{LM}(f_l)T_{MD}(f_s)$$
$$= \frac{1}{4}\left(\sin\frac{\pi x(f_s + f_l)}{c} + \sin\frac{\pi x(f_s - f_l)}{c}\right)^2 \qquad (3)$$

with c the speed of light. The optimum setting of the path length difference x corresponds to the maximum value ($= 1$) of this expression. This setting can easily be found by scanning x since the detected sideband power exhibits a characteristic slow modulation [the second term in Eq. (3)] with period λ_k superimposed upon a fast oscillation [the first term in Eq. (3)] with period $\approx \lambda_l$. An example of such a scan is shown in Fig. 9. The requirement $R = 0.5$ can be closely met if the beams are polarized parallel to the beam splitter foil and if mylar is used as beam splitter material. The thickness of the foil has to be adapted to the wavelength of the radiation to obtain the optimum value of R. The reflection coefficient R is given by the following expression:[37]

$$R = \frac{2r(1 - \cos\delta)}{(1 + r^2) - 2r\cos\delta}, \qquad (4)$$

with

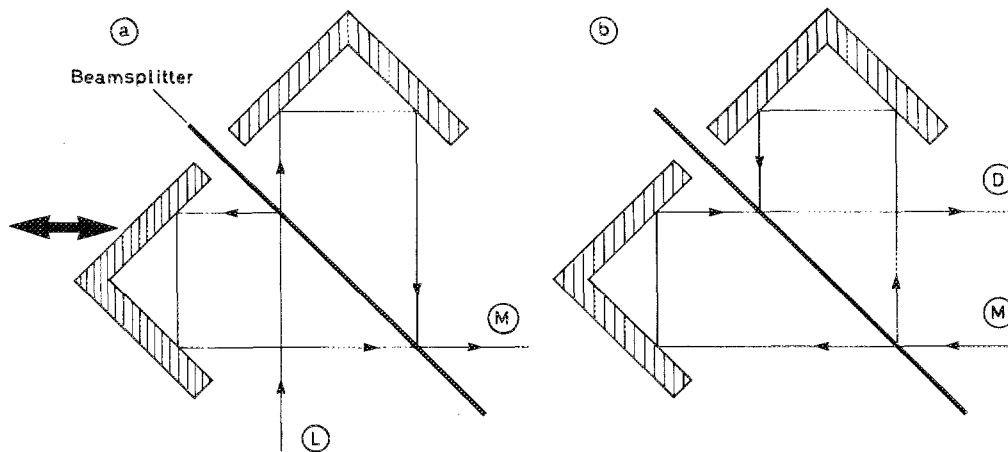$$\delta = \frac{4\pi d}{\lambda}\sqrt{n_b^2 - \frac{1}{2}}$$

and

FIG. 8. Paths of traversal through the ideal diplexer for (a) the FIR laser beam and (b) the sideband beam. The characters L, M, and D refer to laser, mixer, and detector, respectively.

$$r = \left(\frac{\frac{1}{2}\sqrt{2} - \sqrt{n_b^2 - \frac{1}{2}}}{\frac{1}{2}\sqrt{2} + \sqrt{n_b^2 - \frac{1}{2}}} \right)^2,$$

where r is the single pass reflection coefficient at 45° angle of incidence, d is the beam splitter thickness, and n_b is the index of refraction of the beam splitter material ($n_b = 1.7$ for Mylar). The calculated reflection coefficient R is plotted in Fig. 10 for two values of the beam splitter thickness (25 and 50 μm). These two beam splitters are used for laser wavelengths smaller than 230 μm and greater than 230 μm, respectively. In the wavelength region of the present spectrometer, R ranges from 0.43 to 0.34, corresponding to 2%–10% loss of incident laser radiation and about the same amount of leakage of reflected laser radiation to the detector.

B. The monochromator

The imperfect performance of the diplexer demands a further suppression of residual laser radiation. Furthermore, both upper and lower sidebands as well as sidebands with other harmonic numbers n are still in the beam. A grating monochromator is used to select one frequency and obtain a monochromatic beam. It consists of a reflection grating (63 × 63 mm, blaze angle 31°, 3 grooves/mm) and a spherical mirror (24-cm focal length, 15 cm diameter) that focuses the refracted beam on a pinhole. The resulting diverging beam is collimated with a TPX lens (focal length 20 cm). In the present setup the blazed wavelength is 324 μm and the grating is used in first, second, and third order to cover the complete wavelength region 600–100 μm. The use of this monochromator sets an upper wavelength limit of the
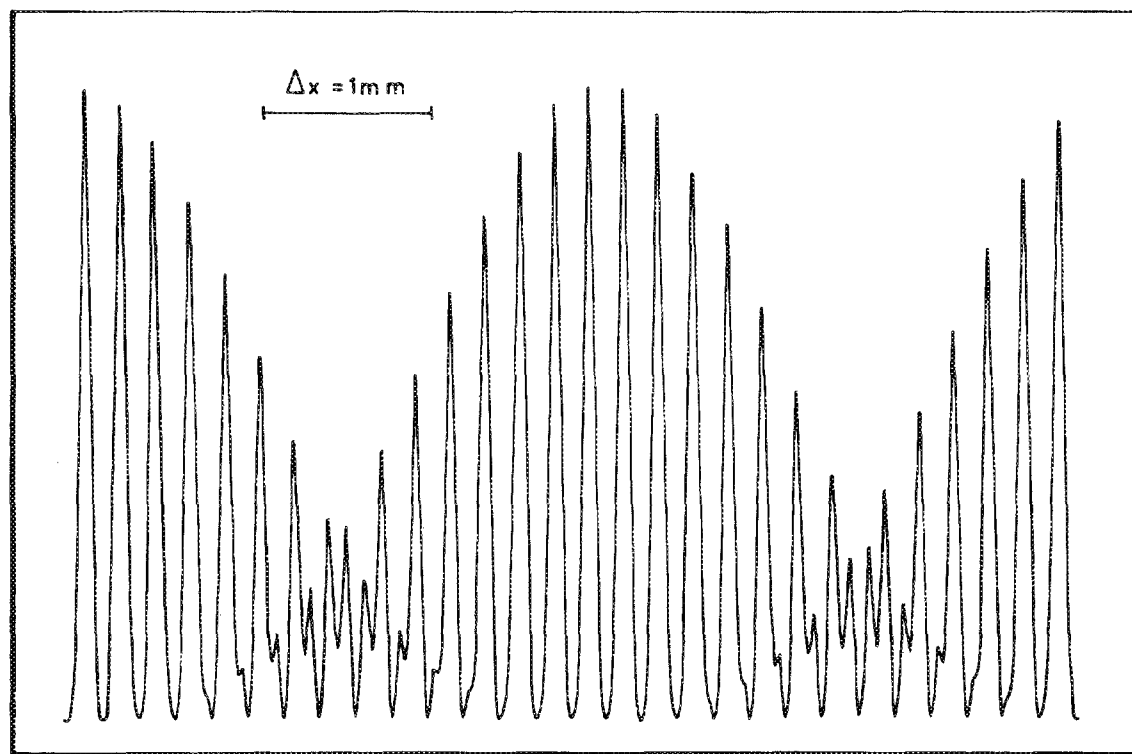

FIG. 9. Sideband signal at the detector vs path difference in the diplexer. $\lambda_l = 214.6$ μm, $\lambda_k = 3.1$ mm, and $\lambda_s = 200.8$ μm.
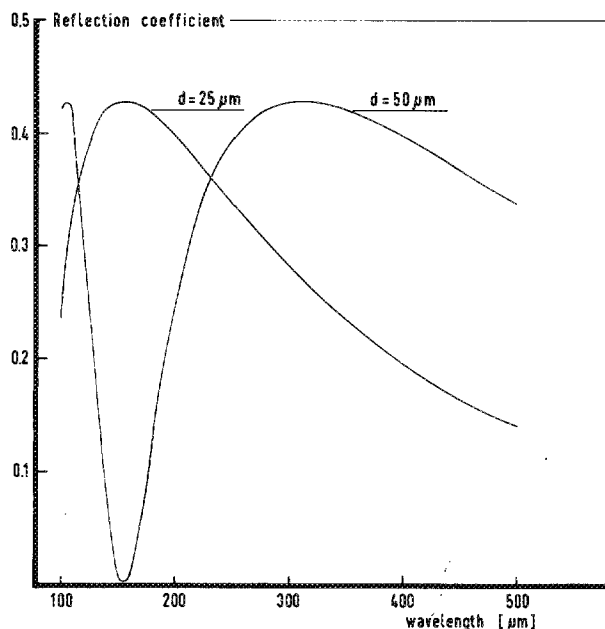
FIG. 10. Calculated reflection coefficient R of Mylar beam splitters (thickness 25 and 50 μm) as a function of wavelength.
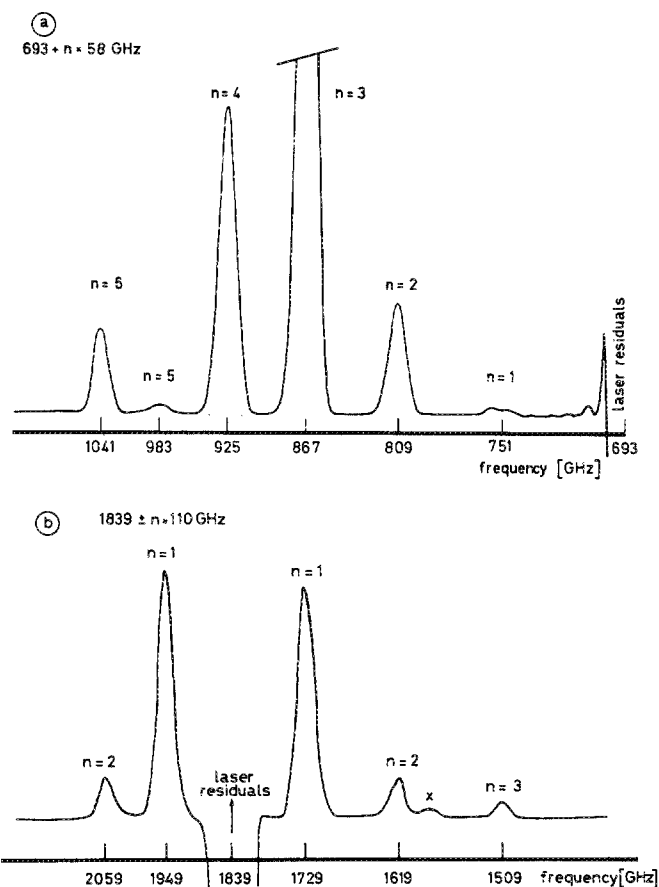

FIG. 11. Simultaneously generated sidebands of order $n = 1$–6, separated with the grating monochromator. (a) laser 693 GHz (HCOOH), klystron 58 GHz. (b) laser 1839 GHz (CH$_3$OH), klystron 110 GHz. (The signal marked with $\times$ is the seventh harmonic frequency of the klystron appearing in first order of the grating.)

spectrometer of about 550 μm.

The calculated resolving power of the grating should allow a separation of two equally intense beams if the difference of their frequencies is more than about 5 GHz, throughout the entire frequency range. In practice, however, the resolution proves to deteriorate towards higher frequencies as can be seen from a comparison of Figs. 11(a) and 11(b), showing monochromator scans at 900 and 1800 GHz. Furthermore, at the entrance of the monochromator, there is still a difference of about two orders of magnitude in the power levels of residual laser radiation and sideband radiation. For an adequate separation of these, the difference in frequency of laser and sideband is therefore kept greater than 20 GHz in the region below 1000 GHz and greater than 50 GHz at higher frequencies.

A drawback of the grating monochromator, compared to Fabry-Perot interferometers used by others,[6,8] is a loss of power of about 50%. The monochromator proves to be, however, very convenient in finding and identifying sidebands.

In normal circumstances, diplexer and monochromator yield sufficient suppression of unwanted radiation. Only in the special case that two or more frequencies are emitted simultaneously by the FIR laser, as is the case for CH$_2$F$_2$ (see Sec. II D), a near coincidence of sideband frequency and unwanted laser frequency might occur. In this case, the unwanted laser emission is suppressed with a Fabry-Perot interferometer positioned just behind the output window of the laser.

V. DETECTION OF SIDEBANDS

The tunable FIR radiation is detected with a He-cooled Ge (composite type) bolometer (Infrared Laboratories),

operated at 1.5 K. Since this instrument can only be used to detect differences in power levels, a modulation of incident radiation is necessary. A convenient way to modulate sideband power is the application of a square-wave modulation to the bias voltage across the Schottky barrier diode. The rather long response time of the bolometer allows only low modulation frequencies (a few hundred Hz). The minimum power that can be detected is determined by the noise equivalent power (NEP) of the system. Taking into account losses in the internal optics of the detector, the efficiency of the bolometer element, and the reduced responsivity at the applied modulation frequency (typically 330 Hz), an effective NEP of 8×10^{-12} W/$\sqrt{\text{Hz}}$ is calculated. This number is almost independent of FIR frequency in the entire region from 600 to 2700 GHz.

VI. LOSSES IN THE SYSTEM

The use of the many optical components necessary to obtain a monochromatic beam of tunable FIR radiation greatly reduces the power level available at the detector. Loss of laser radiation between laser and mixer is due to absorption in one polyethylene lens (thickness 4 mm) and in the mylar beam splitter of the diplexer and due to mismatch
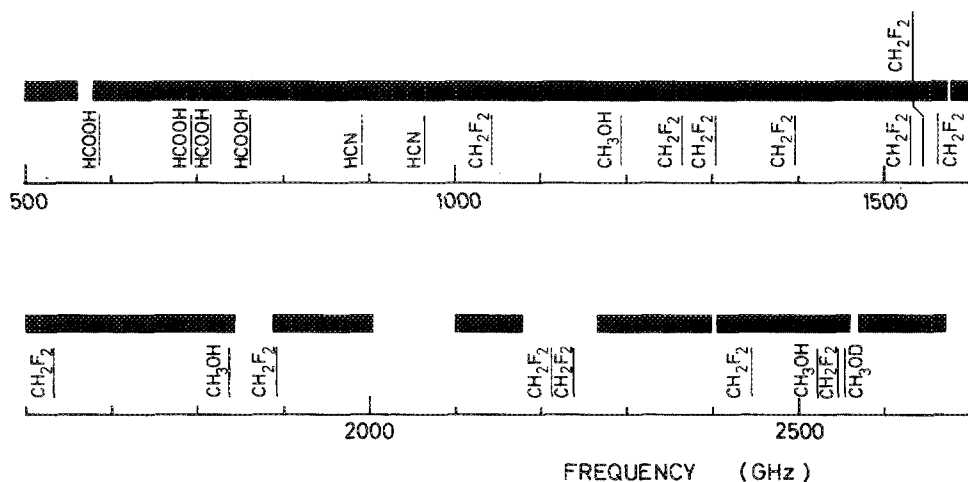
FIG. 12. Frequency range of the spectrometer. The black bars indicate the frequency intervals that are accessible. Laser lines are indicated with vertical sticks and chemical formulae of their gain media. Laser frequencies are listed in Table I.

of the beam splitter thickness (see Sec. IV A). This loss ranges from 20% at 600 GHz to 35% at 2500 GHz. The generated sideband power is attenuated by the beam splitter again (< 10%), the monochromator ($\approx$ 50%), two TPX lenses (thickness 5 mm), and the two polyethylene windows (thickness 4 mm) of the absorption cell used under normal experimental conditions. These losses add up to about 70% at 600 GHz and 85% at 2500 GHz. Gold-coated mirrors used for propagation of the FIR beam are assumed to be lossless in this calculation. Another important loss channel is atmospheric absorption of FIR. Whereas the losses originating from absorption in optical components are more or less constant throughout the entire frequency range, atmospheric absorptions depend strongly on the frequency. They are mainly due to H_2O along the rather long distances between laser and mixer (2 m) and mixer and detector (3.5 m) in the present setup. Especially for frequencies above 1000 GHz this causes severe problems since there are, on the average, three strong absorption lines of H_2O per 100 GHz in this region.[38] These lines are pressure broadened to several GHz. A 50% absorption of sideband power along a path length of 2.5 m has been observed at 10 GHz from the center frequency of a moderately strong water vapor transition ($J_{K_a K_c}$ $= 2_{02} \rightarrow 2_{11}$ at 752 GHz) at normal relative humidity ($\approx$ 60%). A region of 2 GHz was completely "obscured." This problem has been partly overcome by shielding the path of the FIR beam with tubes and boxes. These are flushed with a slow flow of pure nitrogen in order to expel water vapor. At some frequencies this has been observed to increase the sideband power level at the detector by an order of magnitude. Yet, there are still frequencies where no sideband power can be detected due to water vapor absorption.

VII. PERFORMANCE OF THE SPECTROMETER

A. Tunability and sensitivity

From Eq. (1) it follows that several sidebands are generated simultaneously. As described in Sec. IV a single frequency can be selected by means of the diplexer and the monochromator. The individual sidebands can be easily identified with the calibrated monochromator. Examples of the simultaneous generation of sidebands are shown in Figs.

11(a) and 11(b). These are recordings of the bolometer signal when the grating angle and hence the transmitted frequency of the monochromator is scanned. Diplexer and bias voltage across the diode are set to have a reasonable signal on the weakest observable sideband. This yields rather arbitrary relative strengths of the sidebands. Signals were detected phase sensitively by applying a square-wave modulation on the bias voltage. This modulation technique is responsible for the opposite sign of the residual laser signals with respect to the sidebands. Figure 11(a) shows the upper ($f_s > f_l$) series of frequencies generated with the 692.95-GHz laser line of formic acid up to $n = 6$. In this case the $n = 1$ and $n = 5$ bands are nearly coincident with water vapor absorption lines (at 752 and 988 GHz, respectively) and appear weaker than the other bands. Figure 11(b) shows a similar recording in the high frequency range with both upper (up to $n = 2$) and lower (up to $n = 3$) sideband series belonging to the 1838.8-GHz emission of CH_3OH.

For every harmonic number n there is a different dependence on the microwave power coupled to the diode. Therefore the relative strengths of the sidebands of a series also depend on this power. The relative strengths of the individually optimized sidebands that are typically found are 200:20:5:1 for sideband harmonic numbers 1, 2, 3, and 4 in
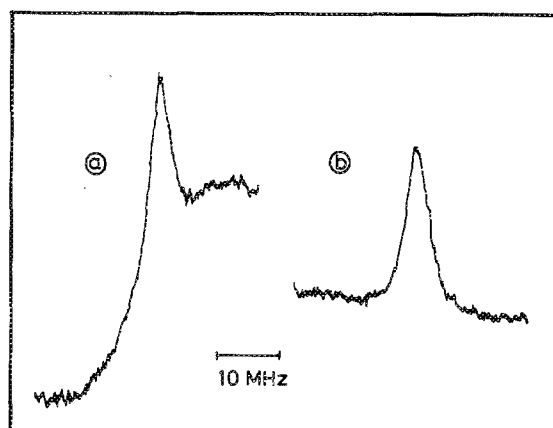

FIG. 13. Reduction of the background variations using a TPX "wobbling" plate. Shown are recordings of the same absorption line without (a) and with (b) this TPX plate in the FIR beam.

Infrared laser spectrometer

case of a strong klystron. For spectroscopic purposes only the bands with $n = 1$ and $n = 2$ are useful because the other frequencies can usually be generated more efficiently with other laser lines. Nevertheless, even the sixth-order sideband in Fig. 11(a) allows detection of molecular absorptions. If only first-order sidebands from the laser lines listed in Table I and the two HCN laser lines are used, about 85% of the frequency range from 500 to 2700 GHz can be covered. The accessible frequency regions are indicated with black bars in Fig. 12.

Typical power levels of tunable far-infrared radiation, generated with the strongest laser lines, are in the microwatt range. In general, a decrease in power with increasing frequency is observed. This is attributed to a somewhat better low-frequency performance of the Schottky barrier diodes, a possible mismatch of the mixer parameters l and d which are difficult to adjust at short wavelengths and to increasing residual atmospheric absorptions at higher frequencies.

Ultimate sensitivity is mainly determined by the noise level of the detector. Only in the low-frequency range (< 1000 GHz), where power levels are relatively high, the noise on the sideband signal, originating from the optically pumped laser, is dominant. The minimum detectable fractional absorptions at time constant $RC = 1$ s and using the strongest laser lines, are 5×10^{-5} up to 1500 GHz and 5×10^{-4} at 2500 GHz. If less sideband power is available at the detector, these numbers are accordingly higher. With the more stable HCN discharge laser, fractional absorptions as low as 10^{-5} can be detected. A decrease in sensitivity may occur in case of baseline fluctuations, due to the phase-sensitive detection technique that is applied. Most spectroscopic investigations performed with this instrument concern molecular ions, produced in a glow discharge. A favorable modulation technique is modulation of the discharge current and thereby of the production of ions. However, the optical pathlength through the discharge is simultaneously modulated due to the change of the index of refraction of the plasma. In combination with interfering reflections between optical components of the spectrometer, this causes a small modulation upon the total sideband signal which appears as a background signal. If the FIR frequency is tuned, this background signal varies more or less periodically, repeating itself after about 40 MHz of change in sideband frequency. This value is only one order of magnitude greater than the typical linewidth of an absorption line [see Fig. 13(a)]. The 40-MHz periodicity implies a distance of 3.7 m between the reflecting surfaces, which is in good agreement with the distance from mixer to detector. The amplitude of the background variations can be as large as 10^{-3} of the total sideband signal.

This problem has been partly solved by inserting a "wobbling" TPX plate (≈ 60 Hz wobbling frequency) in the FIR beam (see Fig. 1). The plate rapidly varies the optical pathlength, yielding an averaged value, and hence smoothes the background variations. A decrease in amplitude of the variations by a factor of five has been achieved in this way [see Figs. 13(a) and 13(b)]. Further suppression is sometimes possible by subtraction of the background signal if signal averaging techniques are used.

The absolute frequency accuracy in a spectroscopic experiment is mainly determined by the uncertainty in the frequency of the FIR laser, which is manually set on top of its gain curve, and is estimated to be 10^{-6} of the laser frequency. A better measurement of the actual laser frequency is possible by beating the laser frequency with a high harmonic signal of a klystron,[39] but this is not performed here in order to avoid complexity of the experiment. Relative frequencies can be determined more accurately since the laser frequency is constant during the time of a scan and the klystron frequency is very well known (see Sec. III A). In this case, Doppler width and flatness of the baseline are the limiting factors. Ultimate frequency resolution depends on the Doppler width of the absorption lines, which is typically 2–10 MHz in this frequency region.

TABLE IV. Observed frequencies of the OD radical ($X^2\Pi$, $v = 0$).

Transition		Observed frequency in MHz	Calculated frequency[a] in MHz	FIR laser frequency in MHz	Gain medium	Harmonic number of sideband
$R_{F_{1,2}}(J)$	parity					
$R_2(1/2)$	$- \leftarrow +$	941 629.3(1.0)	941 630	1 042 $+$ 150.4	CH_2F_2	1
$R_2(1/2)$	$+ \leftarrow -$	944 424.1(1.0)[b]	944 424	890 760.3	HCN	1
$R_1(3/2)$	$+ \leftarrow -$	1 390 620.3(2.0)	1 390 618	1 626 602.6	CH_2F_2	3
$R_1(3/2)$	$- \leftarrow +$	1 391 500.5(2.0)	1 390 498	1 626 602.6	CH_2F_2	3
$R_2(3/2)$	$+ \leftarrow -$	1 567 159.1(2.0)	1 567 158	1 626 602.6	CH_2F_2	1
$R_2(3/2)$	$- \leftarrow +$	1 569 379.9(2.0)	1 569 379	1 626 602.6	CH_2F_2	1
$R_1(5/2)$	$- \leftarrow +$	1 950 599.3(2.0)	1 950 600	1 838 839.3	CH_3OH	1
$R_1(5/2)$	$+ \leftarrow -$	1 952 230.5(2.0)	1 952 232	1 838 839.3	CH_3OH	1
$R_2(5/2)^c$	$- \leftarrow +$	$\cdots$	2 188 199	$\cdots$		
$R_2(5/2)^c$	$+ \leftarrow -$	$\cdots$	2 189 667			
$R_1(7/2)$	$+ \leftarrow -$	2 513 316.3(2.5)	2 513 318	2 447 968.5	CH_2F_2	1
$R_1(7/2)$	$- \leftarrow +$	2 515 798.7(2.5)	2 515 800	2 447 968.5	CH_2F_2	1

[a] From Ref. 40.
[b] From Ref. 30.
[c] Not observed.

B. Spectroscopic applications

The goal of constructing the tunable FIR spectrometer has been the investigation of molecular ions and, in future, of weakly bound molecular complexes. As a first test of the capabilities and limitations of the spectrometer, we looked for the spectra of some relatively easy to detect but astrophysically interesting molecules.

As a first example, we studied the important OD radical in its vibrational and electronic ground state ($X^2 \Pi$). Several rotational transitions have been observed with LMR techniques (listed by Brown et al.[40]), but only one zero-field transition has previously been measured with the precursor of this spectrometer.[30]

The OD radicals were produced in a water-cooled hollow cathode discharge cell designed by van den Heuvel et al.[13] Pure D_2O was discharged at a pressure of 10 Pa and a current of 0.5 A. Due to the paramagnetic nature of the ground state of OD, a splitting of the rotational levels in magnetic sublevels can be induced by small magnetic fields (≈ 4 mT). Application of such a field to the plasma reduces the absorption at the zero-field frequency of a transition. Modulation of the magnetic field (Zeeman modulation) therefore enables phase-sensitive detection of absorption signals. This technique was applied to observe the weaker transitions of OD, whereas the stronger transitions could be observed with an on-off modulation of FIR power (source modulation).

We have observed nine zero-field transitions up to 2.5 THz. These are listed in Table IV together with the calculated frequencies,[40] the laser lines, and the harmonic number of the sideband used. A recording of one of the transitions [$R_2(3/2)$ at 1569.38 GHz] is shown in Fig. 14. In most

cases, hyperfine structure could not be resolved and was only apparent by increased linewidths and asymmetrical line shapes. The hyperfine-free origins of the rotational transitions were estimated with an accuracy of 2 MHz using calculated hyperfine splittings.[41] They are in good agreement with the calculated frequencies.

As a second example we have studied the rotational spectrum of protonated nitrogen, N_2H^+, in its vibrational and electronic ground state. This molecule was initially identified in radio astronomical observations[42,43] and subsequently it was spectroscopically studied in laboratory.[44] Several rotational transitions with low J quantum numbers have been published.[13,44,45]

In our experiment, the N_2H^+ ions are produced in a liquid nitrogen-cooled hollow cathode discharge at a discharge current of 0.5 A. Modulation of the discharge current and hence of the production of the ions was applied and signals were detected phase-sensitively at the modulation frequency (450 Hz). All transitions have been observed in a flowing mixture of H_2 and N_2 at a total pressure of about 7 Pa. The ratio of N_2 to H_2 was not very critical, but the transitions from low J values were best observed with more H_2 than N_2 in the mixture, whereas for high J values the opposite was true. The signals correspond to fractional absorptions of 10^{-1} for $J = 12 \leftarrow 11$ to 8×10^{-3} for $J = 21 \leftarrow 20$. A recording of the latter transition is shown in Fig. 15.

We have observed 13 new transitions involving quantum numbers up to $J = 21$. They are listed in Table V together with the laser lines and harmonic numbers of the sidebands used. A least-squares fit of the observed frequencies, together with previously reported ground-state rotational transitions, was made, using the following expression for the rotational energy levels of a linear molecule like N_2H^+:

$$E(J) = BJ(J+1) - D[J(J+1)]^2, \qquad (6)$$

where B is the rotational constant and D is the centrifugal distortion constant. In the third column of Table V, the observed-calculated frequency differences obtained from this fit are listed. Addition of a sextic centrifugal distortion term in the energy expression of Eq. (6) did not improve the qual-
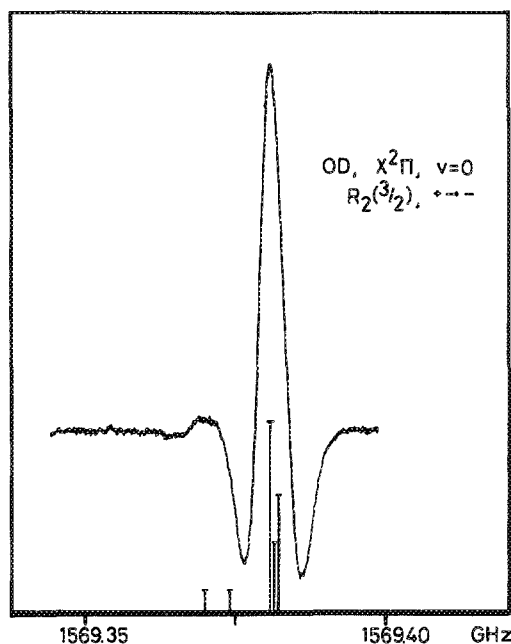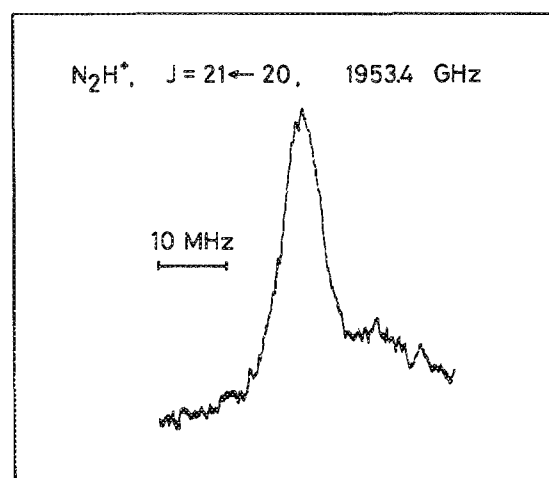

FIG. 14. Recording of a rotational transition of OD with partially resolved hyperfine structure. The sticks represent the calculated hyperfine transitions.[41] The lineshape is due to the Zeeman modulation applied. Time constant was $RC = 1$ s.

FIG. 15. Recording of the highest observed rotational transition of N_2H^+ ($RC = 10$ s).

Infrared laser spectrometer

TABLE V. Observed frequencies of N_2H^+.

$J' \leftarrow J''$	Observed frequency in MHz	obs-cal	FIR laser frequency in MHz	Gain medium	Harmonic number of sideband
$6 \leftarrow 5$	558 965.7(1.0)	− 0.8	761 607.7	HCOOH	2
$7 \leftarrow 6$	652 094.7(1.0)	− 0.9	761 607.7	HCOOH	1
$8 \leftarrow 7$	745 209.6(1.0)	− 0.3	964 312.7	HCN	2
$9 \leftarrow 8$	838 307.1(1.0)	− 0.3	761 607.7	HCOOH	1
$10 \leftarrow 9$	931 386.2(1.0)	+ 0.4	1 042 150.4	CH_2F_2	1
$11 \leftarrow 10$	1 024 443.2(1.0)	+ 0.0	964 312.7	HCN	1
$12 \leftarrow 11$	1 117 477.1(1.2)	− 0.2	1 193 727.3	CH_3OH	1
$13 \leftarrow 12$	1 210 486.9(1.4)	+ 0.7	1 397 118.6	CH_2F_2	2
$14 \leftarrow 13$	1 303 467.8(1.4)	+ 0.2	1 397 118.6	CH_2F_2	1
$15 \leftarrow 14$	1 396 421.2(2.0)	+ 2.0	1 300 334.3	CH_2F_2	1
$16 \leftarrow 15$	1 489 338.9(1.4)	− 0.7	1 397 118.6	CH_2F_2	1
$17 \leftarrow 16$	1 582 225.1(1.4)	− 1.0	1 397 118.6	CH_2F_2	2
$18 \leftarrow 17^a$	...		...		
$19 \leftarrow 18$	1 767 889.7(1.8)	+ 0.4	1 838 839.3	CH_3OH	1
$20 \leftarrow 19^a$	...		...		
$21 \leftarrow 20$	1 953 392.3(1.8)	+ 0.1	1 838 839.3	CH_3OH	1

[a] Not observed.

ity of the fit. The resulting parameters B and D are $B = 46\,586.8738(5)$ MHz and $D = 0.087\,910(4)$ MHz, in agreement with those obtained by Foster and McKellar[46] from a fit of six ground-state rotational frequencies and 22 rovibrational frequencies from the fundamental band of the v_3 vibration. The numbers in parentheses represent one standard deviation in units of the last quoted digit.

Recently we have observed the ground-state inversion spectrum of the hydronium ion H_3O^+ at 1600 GHz. Results of this investigation have been reported elsewhere.[14]

ACKNOWLEDGMENTS

[1] P. Helminger, J. K. Messer, and F. C. De Lucia, Appl. Phys. Lett. **42**, 309 (1983).

[2] S. P. Belov, L. I. Gershstein, A. F. Krupnov, A. V. Maslovsky, V. Špirko, and D. Papoušek, J. Mol. Spectrosc. **84**, 288 (1980).

[3] D. D. Bicanic, B. F. J. Zuidberg, and A. Dymanus, Appl. Phys. Lett. **32**, 367 (1978).

[4] W. A. M. Blumberg, H. R. Fetterman, D. D. Peck, and P. F. Goldsmith, Appl. Phys. Lett. **35**, 582 (1979).

[5] H. Kräutle, E. Sauter, and G. V. Schultz, Infrared Phys. **17**, 477 (1977).

[6] J. Farhoomand, G. A. Blake, M. A. Frerking, and H. M. Picket, J. Appl. Phys. **57**, 1763 (1984).

[7] P. Verhoeve, J. J. ter Meulen, W. L. Meerts, and A. Dymanus, Chem. Phys. Lett. **125**, 286 (1986).

[8] R. C. Cohen, K. L. Busarow, K. B. Laughlin, G. A. Blake, M. Havenith, Y. T. Lee, and R. J. Saykally, J. Chem. Phys. **89**, 4494 (1988).

[9] G. Piau, F. X. Brown, D. Dangoisse, and P. Glorieux, IEEE J. Quantum Electron. **QE-23**, 1388 (1987).

[10] K. M. Evenson, D. A. Jennings, and F. R. Petersen, Appl. Phys. Lett. **44**, 576 (1984).

[11] D. A. Jennings, K. M. Evenson, L. R. Zink, C. Demuynck, J. L. Destombes, B. Lemoine, and J. W. C. Johns, J. Mol. Spectrosc. **122**, 477 (1987).

[12] F. X. Brown, Ph. D. Thesis, Universite des Sciences et Techniques de Lille, Lille, France, 1988.

[13] F. C. van den Heuvel and A. Dymanus, Chem. Phys. Lett. **92**, 219 (1982).

[14] P. Verhoeve, M. Versluis, J. J. ter Meulen, W. L. Meerts, and A. Dymanus, Chem. Phys. Lett. **161**, 195 (1989).

[15] D. D. Bicanic and A. Dymanus, Infrared Phys. **14**, 153 (1974).

[16] T. Y. Chang and T. J. Bridges, Opt. Commun. **1**, 423 (1970).

[17] D. T. Hodges and T. S. Hartwick, Appl. Phys. Lett. **23**, 252 (1973).

[18] F. Strumia., I. Ioli, and A. Moretti, in *Physics of New Laser Sources*, edited by N. B. Abraham, F. T. Arecchi, A. Mooradian, and A. Sona (NATO ASI Series, Plenum, New York, 1985), Vol. 132.

[19] D. J. E. Knight, NPL Report QU 45 (first revision), National Physics Laboratory, Teddington, UK (1982).

[20] R. L. Abrams, IEEE J. Quantum Electron. **QE-8**, 838 (1972).

[21] E. A. J. Marcatili and R. A. Schmeltzer, Bell Syst. Tech. J. **43**, 1782 (1964).

[22] D. T. Hodges, F. B. Foote, and R. D. Reel, IEEE J. Quantum Electron. **QE-13**, 491 (1977).

[23] D. T. Hodges, F. B. Foote, and R. D. Reel, Appl. Phys. Lett. **29**, 662 (1976).

[24] J. W. C. Johns, J. Opt. Soc. Am. B **2**, 1340 (1985).

[25] J-L. Lachambre, P. Bernard, and M. Gagne, IEEE J. Quantum Electron. **QE-21**, 282 (1985).

[26] B. W. Davis and A. Vass, Int. J. Infrared Mm Waves **9**, 279 (1988).

[27] D. J. E. Knight, K. I. Pharaoh, and M. J. Padgett, Sov. J. Quantum Electron. **18**, 753 (1988).

[28] E. Hirota, J. Mol. Spectrosc. **69**, 409 (1978).

[29] E. J. Danielewicz, in *Review of IR-MM Waves*, edited by K. J. Button, M. Inguscio, and F. Strumia (Plenum, New York, 1984), Vol. 2.

[30] F. C. van den Heuvel, Ph.D. Thesis, Katholieke Universiteit, Nijmegen, 1982.

[31] H. Jasik, *Antenna Engineering Handbook* (McGraw-Hill, New York 1961).

[32] L. M. Matarrese and K. M. Evenson, Appl. Phys. Lett. **17**, 8 (1970).

[33] H. Kräutle, E. Sauter, and G. V. Schultz, Infrared Phys. **18**, 705 (1978).

[34] B. J. Clifton, IEEE Trans. Microwave Theory Tech. **MTT-25**, 457 (1977).

[35] A. Sanchez, S. K. Singh, and A. Javan, Appl. Phys. Lett. **21**, 240 (1972).

[36] N. R. Erickson, IEEE Trans. Microwave Theory Tech. **MTT-25**, 865 (1977).

[37] E. Hecht and A. Zajac, *Optics* (Addison-Wesley, Reading, MA, 1973).

[38] R. T. Hall and J. M. Dowling, J. Chem. Phys. **47**, 2454 (1976).

[39] F. C. van den Heuvel, W. L. Meerts, and A. Dymanus, J. Mol. Spectrosc. **84**, 162 (1980).

[40] J. M. Brown, J. E. Schubert, C. E. Brown, J. S. Geiger, and D. R. Smith, J. Mol. Spectrosc. **114**, 185 (1985).

[41] J. M. Brown and J. E. Schubert, J. Mol. Spectrosc. **95**, 194 (1982).

[42] B. E. Turner, Astrophys. J. **193**, L83 (1974).

[43] P. Thaddeus and B. E. Turner, Astrophys. J. **201** L25 (1975).

[44]R. J. Saykally, T. A. Dixon, T. G. Anderson, P. G. Szanto, and R. C. Woods, Astrophys. J. 205, L101 (1976).

[45]K. V. L. N. Sastry, P. Helminger, E. Herbst, and F. C. De Lucia, Chem. Phys. Lett. 84, 286 (1981).

[46]S. C. Foster and A. R. W. McKellar, J. Chem. Phys. 81, 3424 (1984).

[47]F. R. Petersen, A. Scalabrin, and K. M. Evenson, Int. J. Infrared Mm Waves 1, 111 (1980).